ACS APPLIED MATERIALS & INTERFACES

www.acsami.org

Research Article

Ultrastable and Redispersible Zwitterionic Bottlebrush Micelles for Drug Delivery

Jeonghun Lee, Yao Tang, Karla E. Cureño Hernandez, Sunghoon Kim, Rahmi Lee, Zachary Cartwright, Darrin J. Pochan, and Margarita Herrera-Alonso*

Cite This: *ACS Appl. Mater. Interfaces* 2024, 16, 55118–55129

Read Online

ACCESS | Metrics & More | Article Recommendations | Supporting Information

ABSTRACT: Bottlebrush copolymers are increasingly used for drug delivery and biological imaging applications in part due to the enhanced thermodynamic stability of their self-assemblies. Herein, we discuss the effect of hydrophilic block chemistry on the stability of bottlebrush micelles. Amphiphilic bottlebrushes with zwitterionic poly(2-methacryloyloxyethyl phosphorylcholine) (PMPC) and nonionic polyethylene glycol (PEG) hydrophilic blocks were synthesized by "grafting from" polymerization and self-assembled into well-defined spherical micelles. Colloidal stability and stability against disassembly were challenged under high concentrations of NaCl, $MgSO_4$, sodium dodecyl sulfate, fetal bovine serum, and elevated temperature. While both types of micelles appeared to be stable in many of these conditions, those with a PMPC shell consistently surpassed their PEG analogs. Moreover, when repeatedly subjected to lyophilization/resuspension cycles, PMPC micelles redispersed with no apparent variation in size or dispersity even in the absence of a cryoprotectant; PEG micelles readily aggregated. The observed excellent stability of PMPC micelles is attributed to the low critical micelle concentration of the bottlebrushes as well as to the strong hydration shell caused by ionic solvation of the phosphorylcholine moieties. Zwitterionic micelles were loaded with doxorubicin, and higher loading capacity/efficiency, as well as delayed release, was observed with increasing side-chain length. Finally, hemocompatibility studies of PMPC micelles demonstrated no disruption to the red blood cell membranes. The growing concern regarding the immunogenicity of PEG-based systems propels the search for alternative hydrophilic polymers; in this respect and for their outstanding stability, zwitterionic bottlebrush micelles represent excellent candidates for drug delivery and bioimaging applications.

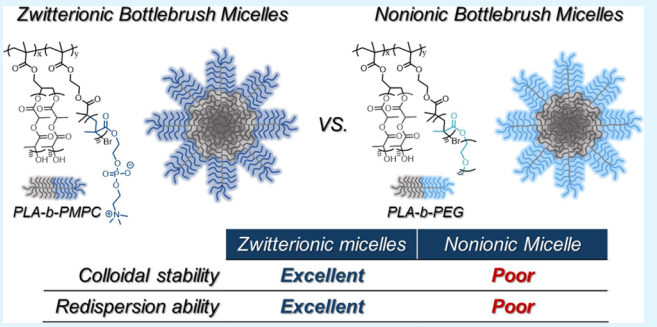

KEYWORDS: *zwitterionic polymers, amphiphilic bottlebrushes, drug delivery, ultrastable nanoparticles, redispersible nanoparticles*

INTRODUCTION

Macromolecular brushes, or bottlebrushes, are a class of polymers with a unique, highly branched architecture for which side-chain length exceeds graft spacing. Their architectural complexity translates into intramolecular excluded volume effects that cause long backbones to adopt a persistent cylindrical shape with radially emanating side chains, influencing their physicochemical properties.[1−5] As building blocks for nanomaterials fabrication, bottlebrushes enable the formation of nanostructures with shapes, sizes, and periodic morphologies that are inaccessible from linear polymers, ranging from tens to hundreds of nanometers.[6−11] Depending on the relative placement and types of comonomers used for their synthesis, bottlebrushes have been explored as unimolecular constructs or as building blocks of multimolecular assemblies.

Bottlebrush block copolymers have been shown to self-assemble into spherical, cylindrical, and bilayer structures.[7,12−16] The interfacial curvature of the resulting self-assemblies is largely dictated by side-chain asymmetry between the two blocks and influences micelle aggregation number, morphology, and surface roughness.[13,17] Nanoparticles from bottlebrush block copolymers are of particular interest for drug delivery and biological imaging applications[18,19] as shown in the development of carriers for chemotherapeutics or theranostics,[17,20−22] or micellar-based injectable hydrogels.[23] The ability to modulate nanoparticle dimensions based on simple molecular parameters is advantageous for the design of drug carriers, as sizes must be tailored between 6 and 200 nm to avoid renal clearance, reduce opsonization, and preclude clearance by the reticuloendothelial system.[18,24] Nanoparticle stability is another important design parameter for delivery applications, as disassembly upon high dilution can lead to

Received: July 2, 2024
Revised: September 24, 2024
Accepted: September 30, 2024
Published: October 7, 2024

reduced therapeutic efficacy, as observed for small-molecule amphiphiles or linear amphiphilic diblock copolymers. Amphiphilic diblock bottlebrushes exhibit critical micelle concentrations (C_{CMC}) considerably lower than their analogous linear diblock copolymers—on occasions, an order of magnitude lower—resulting in self-assemblies with high thermodynamic stability.[13,15] Ensuring colloidal stability in biological media is equally paramount to preventing aggregation or the cascade of undesirable events that arise from protein corona formation. Stabilization against disassembly has been studied for a variety of micelles from linear polymeric amphiphiles, primarily through the formation of permanent (nondegradable) covalent bonds, although more recent approaches have focused on reversible cross-linkable moieties for additional responsiveness.[25−33] Far fewer examples of cross-linked bottlebrush assemblies exist.[20]

While poly(ethylene glycol) has been the hydrophilic component of choice for the majority of amphiphilic bottlebrushes to date, there is increasing concern regarding accumulated toxicity, autoxidation, and immunogenicity associated with PEG-based systems.[34−38] In this sense, zwitterionic polymers emerge as alternatives to PEG,[39] exhibiting unique antibiofouling and cryoprotective properties, largely attributed to the strong hydration layer caused by ionic solvation of their highly charged—yet net neutral—functionalities.[40−46] The capacity of zwitterionic polymer-coated surfaces to resist nonspecific protein adsorption and inhibit ice formation and growth are of great biomedical interest, as these properties could lead to nanoparticles with enhanced stability in serum and resistance to lyophilization and redispersion without the need for cryoprotectant agents.

Herein, we report on the synthesis of amphiphilic zwitterionic bottlebrush copolymers and their self-assembled structures. We challenged nanoparticle stability against disassembly and colloidal stability under high concentrations of surfactant and extreme ionic strength conditions and contrasted the observed behavior to a PEG-based system. Finally, we examine the suitability of zwitterionic bottlebrush micelles as drug delivery vehicles by evaluating their colloidal stability in the presence of fetal bovine serum, their hemolysis, and their ability to encapsulate the chemotherapeutic doxorubicin. We attribute the observed enhanced stability and redispersibility of zwitterionic bottlebrush micelles to the strong hydration layer of the hydrophilic block, making them excellent platforms for bioimaging and drug delivery applications.

EXPERIMENTAL SECTION

Materials. All chemicals and solvents were commercially available and purchased from Fisher Scientific, TCI, and Sigma-Aldrich unless otherwise mentioned. 2-Cyano-2-propyl benzodithioate (CPB) was purchased from Angina Chemical. (2-Methacryloyloxyethyl phosphorylcholine) (MPC) was purchased from Ambeed. D,L-Lactide and 2,2-Azobis(2-methylpropionitrile) (AIBN) were recrystallized from ethyl acetate and methanol, respectively. 1,8-Diazabicyclo[5.4.0]-undec-7-ene (DBU) was dried over molecular sieves (3 Å) overnight. Glycidyl methacrylate (GMA) was passed through basic alumina to remove the inhibitors immediately before polymerization.

Instrumentation. ^{1}H NMR and ^{13}C NMR spectra were acquired on a Bruker NEO 400 MHz spectrometer equipped with a prodigyTM BBFO probe in $CDCl_3$, DMSO-d_6, and MeOD-d_4, as noted in each spectrum. GPC analysis was carried out at 40 °C on a Waters 1515 Isocratic HPLC equipped with two Styragel columns (HR3 and HR4, 300 mm × 7.8 mm) connected in series and refractive index and ultraviolet detectors. The mobile phase used was 2,2,2-trifluoroethanol (TFE) with 10 mM sodium trifluoroacetate. Poly(methyl methacrylate) (PMMA) standards were used for calibration. Dynamic light scattering (DLS) analysis was conducted on a Malvern Instruments Nano-ZS ZetaSizer at 633 nm with a scattering angle of 173°. Fluorescence data was collected with an Edinburgh FS5 spectrofluorometer with a 150 W xenon lamp. Excitation and emission bandwidths were set to 2 nm. Transmission electron microscopy (TEM) images were collected on a JEOL JEM-2100F transmission electron microscope operated at an acceleration voltage of 200 kV. Samples were dropped on a carbon-coated copper grid (Electron Microscopy, Hatfield, PA) and stained with 2 wt % aqueous uranyl acetate solution. Cryogenic-transmission electron microscopy (Cryo-TEM) images were acquired on an FEI TALOS F200C microscope with an accelerating voltage of 200 kV. All images were captured with a 4k × 4k FEI Ceta 16 M camera.

Synthesis of 2-((2-Bromo-2-methylpropanoyl)oxy)ethyl Methacrylate (BIEM). BIEM was synthesized following a modified version of a previously published protocol.[47] Hydroxyethyl methacrylate (10.0 mL, 82.2 mmol), triethylamine (16.4 mL, 117.5 mmol), and anhydrous dichloromethane (250 mL) were placed in a 500 mL round-bottomed flask equipped with a stir bar and capped with a septum. The mixture was cooled in an ice bath for 30 min and stirred vigorously during the addition of 2-bromoisobutyryl bromide (9.68 mL, 78.30 mmol), which was introduced dropwise via a syringe pump. A white precipitate was observed during the injection. After 1 h, the ice bath was removed and the reaction was continued for 12 h at room temperature. The resulting white solid was removed by vacuum filtration, and a clear yellowish organic solution was collected. The mixture was washed with 1 M HCl (300 mL × 3), DI water (300 mL × 3), and brine (300 mL × 3). The organic mixture was then dried with magnesium sulfate and concentrated by rotary evaporation. The resulting viscous oil was purified by column chromatography with ethyl acetate:hexane (1:2) as an eluent, yielding a yellowish oil (89% yield). ^{1}H NMR (400 MHz, DMSO-d_6) δ (ppm): 6.08 (s, 1H), 5.73 (m, 1H), 4.42 (m, 2H), 4.40 (m, 2H) 1.91 (s, 9H). ^{13}C NMR (DMSO-d_6) δ (ppm): 171.10, 166.74, 136.06, 126.49, 63.90, 62.37, 57.24, 30.70, 18.34.

Synthesis of Poly(glycidyl Methacrylate), $PGMA_{103}$ (B1). Glycidyl methacrylate (5 mL, 36.7 mmol), CPB (73.8 mg, 0.3 mmol), and anhydrous dioxane (9 mL) were loaded into a 25 mL Schlenk flask equipped with a stir bar and capped with a septum. A solution of AIBN in dioxane (10 mg/mL) was then added (501.5 μL, 33.3 μmol), and the resulting mixture was bubbled with argon at room temperature for 30 min. The flask was immersed in an oil bath at 70 °C and the reaction was carried out for 16 h with continuous stirring. The polymerization was then quenched by opening the flask to the atmosphere and cooling the mixture in an ice bath. An aliquot was collected to determine monomer conversion by ^{1}H NMR. The mixture was diluted with tetrahydrofuran and precipitated in cold methanol three times. The resulting pink powder was dried under a vacuum for 24 h (80% yield). ^{1}H NMR (400 MHz, DMSO-d_6): M_n = 14.9 kg/mol (93.3% conversion, 103 repeat units). GPC: $Đ$ = 1.10.

Synthesis of Poly(GMA_{103}-*b*-$BIEM_{105}$): Polymerization and Removal of the CTA (B2 and B3). $PGMA_{103}$ (500 mg, 33.6 μmol) and BIEM (1.221 g, 4.4 mmol) were completely dissolved into anhydrous dioxane (6 mL) inside a Schlenk flask equipped with a stir bar and capped with a septum for 30 min with vigorous stirring. A solution of AIBN in dioxane (10 mg/mL) was subsequently injected into the flask (10.5 μL, 6.73 μmol). The mixture was degassed by bubbling with argon for 30 min. The flask was immersed in an oil bath at 70 °C and the polymerization was carried out for 16 h with continuous stirring. The polymerization was then quenched by opening the flask to the atmosphere and cooling the mixture in an ice bath. An aliquot was collected to determine monomer conversion by ^{1}H NMR. The viscous solution was diluted with dichloromethane and precipitated in cold methanol three times. The polymer was dried under a vacuum for 24 h to yield a slightly pink powder (75% yield). ^{1}H NMR (400 MHz, DMSO-d_6): M_n = 44.2 kg/mol (81% conversion, 105 repeat units). GPC: $Đ$ = 1.11. Poly(GMA_{103}-*b*-

https://doi.org/10.1021/acsami.4c10968
ACS Appl. Mater. Interfaces 2024, 16, 55118−55129

$BIEM_{105}$) (1.0 g, 22.6 μmol) and AIBN (92.9 mg, 566.0 μmol) were dissolved in 5 mL of dry dioxane in a 25 mL round-bottomed flask equipped with a stir bar and capped with a septum. After all solids were dissolved, the solution was bubbled with argon for 30 min, and the flask was then placed in an oil bath at 75 °C. After 3 h, the mixture was cooled to 0 °C and precipitated in cold hexane three times. A white solid was recovered and dried overnight under vacuum (85% yield). CTA removal was confirmed by ^{1}H NMR. ^{1}H NMR (400 MHz, DMSO-d_6): M_n = 44.1 kg/mol. GPC: $Đ$ = 1.15.

Hydrolysis of Poly(GMA_{103}-*b*-$BIEM_{105}$) (B4). Poly(GMA_{103}-*b*-$BIEM_{105}$) (800 mg, 18.2 μmol) was dissolved in dimethylformamide (7 mL) with vigorous stirring for 30 min in a 25 mL round-bottom flask. Subsequently, 2 mL of 1 M HCl was added dropwise over 30 min. After 18 h, the solution was transferred to a 6−8 kDa dialysis membrane (Spectrum Spectra/Por) and dialyzed against a mixture of methanol/acetone (1:1 v/v) for 24 h. After this time, the medium was switched to Nanopure water for 24 h, and the resulting suspension was lyophilized (90% yield). ^{1}H NMR (400 MHz, DMSO-d_6): M_n = 45.9 kg/mol. GPC: $Đ$ = 1.15.

Synthesis of poly((GMA_{103}-*g*-LA_x)-*b*-$BIEM_{105}$). Hydrolyzed poly(GMA_{103}-*b*-$BIEM_{105}$) and D,L-lactide were loaded into a Schlenk flask equipped with a magnetic stir bar and a septum and placed under high vacuum at 40 °C for 3 h. After backfilling with argon, anhydrous DMF was injected into the flask to dissolve the reagents and the mixture was stirred at room temperature for 1 h. DBU was introduced via a syringe to initiate the polymerization and the reaction was allowed to proceed under argon at room temperature for 2 h. Then, a solution of benzoic acid was introduced to quench the reaction. An aliquot was taken to determine monomer conversion by ^{1}H NMR. The viscous solution was directly precipitated into cold methanol three times to obtain a white solid. The resulting polymer was dried under a vacuum in an oven for 24 h prior to characterization by ^{1}H NMR and GPC. Details of the synthesis are provided in Table S1.

Synthesis of Poly((GMA_{103}-*g*-LA_x)-*b*-($BIEM_{105}$-*g*-$PMPC_y$)) (ZBCPs). Poly((GMA_{103}-*g*-LA_x)-*b*-$BIEM_{105}$) and MPC were loaded into a Schlenk flask equipped with a stir bar and a septum and completely dissolved in a mixture of DMF/MeOH (1:1 v/v) for 30 min at room temperature. Then, a solution of TPMA in DMF and a solution of ascorbic acid in DMF were added to the flask and the reaction mixture was degassed by bubbling with argon for 30 min. A degassed solution of $CuBr_2$ in DMF was then injected into the flask to initiate the polymerization of MPC. The reaction was carried out for 18 h at room temperature, and aliquots were collected at different time points to monitor monomer conversion. After this time, the resulting solutions were loaded into 50 kDa dialysis bags (Spectrum Spectra/Por) and dialyzed against a mixture of methanol/acetone (1:1 v/v) for 2 days. The dialyzed solutions were concentrated by rotary evaporation, and the transparent films that resulted were dried inside a vacuum oven overnight. Details of the synthesis are provided in Table S2.

Synthesis of Poly((GMA_{103}-*g*-LA_9)-*b*-($BIEM_{105}$-*g*-PEG_{11})) (NBCP). A PEG-based equivalent of ZBCP was synthesized following the same procedure as above with two exceptions. The first is that the polymerization was carried out in DMF rather than DMF/MeOH, and the second is that the polymer was purified by precipitation into cold diethyl ether (3×) rather than by dialysis. Details of the synthesis are provided in Table S2.

Critical Micelle Concentration (C_{CMC}). A detailed protocol to determine critical micelle concentrations of all copolymers was previously described.[48] In brief, a stock solution of pyrene in acetone was prepared at a concentration of 6.0×10^{-5} M. DI water (1 mL) was then added dropwise to scientific vials containing polymer films. The final polymer concentration ranged from 0.05 μg/mL to 1 mg/mL, whereas the concentration of pyrene was maintained constant for all samples (6.0×10^{-7} M). Pyrene excitation was recorded from 300 to 360 nm with an emission wavelength of 390 nm. The intensity ratio from signals at 336 and 334 nm (I_{336}/I_{334}) was recorded and plotted as a function of polymer concentration.

Preparation of Unloaded and DOX-Loaded Micelles. Micelles were prepared according to a direct dissolution method. Unloaded micelles were prepared as follows. A stock solution of the block copolymer in 2,2,2-trifluoroethanol (TFE) was initially prepared at room temperature (10 mg of polymer/mL TFE). 500 μL of the stock solution was added to a 20 mL scientific vial. The solvent was completely removed by rotary evaporation under heat (65 °C) to produce thin films. Nanopure water (5 mL) was then added to each vial to achieve a final polymer concentration of 1 mg/mL. Self-assembly was carried out by a brief bath sonication at 65 °C for 7 min. The resulting micelles were filtered through a 0.45 μm PVDF syringe filter (Thermo Scientific) and stored in 5 mL clean scientific vials for further experiments. Micelles loaded with doxorubicin (DOX) were prepared by following a similar procedure. A stock solution of DOX (1 mg/mL in TFE) was prepared. 500 μL of the polymer stock solution and 500 μL of the DOX stock solution were added to scientific vials (20 mL) and the solvent was completely removed by rotary evaporation, yielding thin films. Subsequent steps were followed as described above. Micelle morphology, size, and size distribution were determined by cryo-TEM, TEM, and DLS.

Colloidal Stability and Stability against Disassembly. This was assessed by four independent experiments: stability in the presence of sodium dodecyl sulfate, stability in solutions of high ionic strength, thermal stability, and stability in the presence of fetal bovine serum (FBS). For these experiments, micelle suspensions were prepared following the direct dissolution method described above, adjusting the final polymer concentration to 2 mg/mL. Then, 1 mL of micelle suspension and 1 mL of 2× buffer solution were mixed to yield final micelle and buffer concentrations of 1 mg/mL and 1×, respectively. The buffers utilized to examine micellar stability under each of these conditions consisted of the following: (i) for stability in the presence of sodium dodecyl sulfate: 10 mg/mL SDS in water; (ii) for stability in solutions of high ionic strength: 2 M NaCl, 2 M $MgSO_4$, 2 M NaCl + 2 M $MgSO_4$; (iii) for stability in the presence of FBS: 2× PBS, and 2× PBS + 20% FBS. Average micelle size and dispersity were measured by DLS over 14 days. In the case of thermal stability, average micelle size and dispersity were measured by DLS at 25 and 70 °C for 10 cycles. Micelle concentration was 1 mg/mL for this experiment.

Micellar Reconstitution. Three mL of micelle suspension (1 mg/mL) were transferred to a scintillation vial and frozen by submersion into liquid nitrogen for 10 min prior to lyophilization for 48 h at −52 °C. The resulting powder was rehydrated with 3 mL of nanopure water and mixed using a vortex mixer at 2500 rpm for 40 s. This process (lyophilization/rehydration) was repeated 5 times for unloaded micelles. The resulting suspensions were examined by TEM and DLS.

Drug Loading Capacity (DLC) and Drug Loading Efficiency (DLE) of DOX-Loaded Micelles. Drug loading capacity and efficiency were measured for DOX-loaded lyophilized micelles.[49] For this, lyophilized micelles were dissolved in TFE and the fluorescence intensity of the solution was measured at 470 nm excitation wavelength and 590 nm emission wavelength. The amount of doxorubicin was quantified from a standard curve.

Doxorubicin Release Profiles. In vitro doxorubicin release was measured by dialysis methods.[50,51] For this, 5 mL of DOX-loaded micelle suspension (1 mg/mL) was loaded into a dialysis bag (MWCO 6−8 kDa, Spectrum Spectra/Por). Suspensions were dialyzed against 40 mL of PBS solution with Tween-20 (1% v/v%) under constant stirring at 500 rpm and 37 °C. Aliquots (2 mL) were taken at predetermined time points from the medium and replaced with fresh medium (2 mL) to maintain the total medium volume constant (40 mL). The fluorescence intensity of the solution was measured at 470 nm excitation and 590 nm emission wavelength. The amount of doxorubicin was quantified from a standard curve. Values are plotted as the averages of three independent replicates.

Hemolysis Assay. The protocol for the hemolysis assay was previously reported.[52,53] Briefly, fresh ethylenediamine tetraacetic acid (EDTA)-stabilized mouse whole blood samples were collected from C57BL6 mice (12 weeks old). 1.5 mL of whole blood was added to a 15 mL conical tube filled with Dulbecco's phosphate-buffered saline (DPBS) without calcium and magnesium (1× DPBS, Manassas, VA)

https://doi.org/10.1021/acsami.4c10968
ACS Appl. Mater. Interfaces 2024, 16, 55118−55129

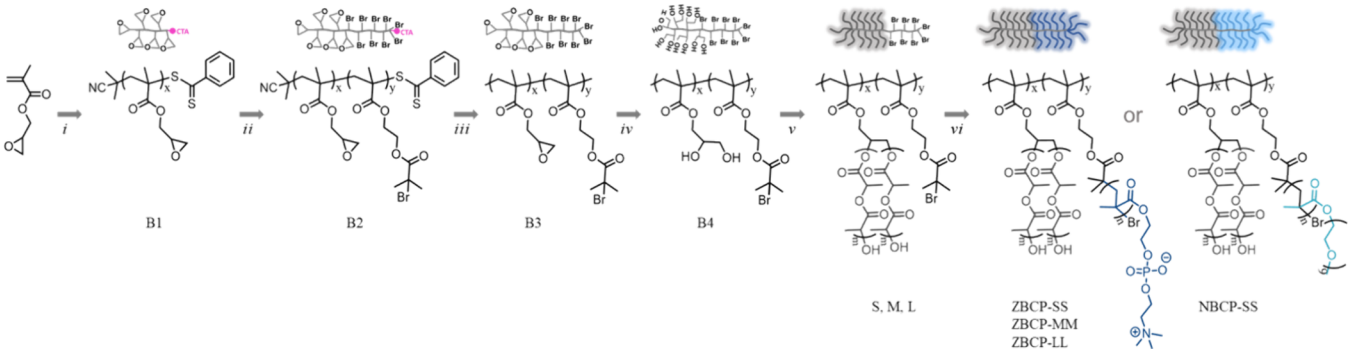

Figure 1. Synthesis protocol of zwitterionic bottlebrush copolymers (ZBCPs) and nonionic bottlebrush copolymer (NBCP). (i) AIBN, CTA, dioxane, 65 °C, 18 h; (ii) AIBN, BIEM, dioxane, 70 °C, 16 h; (iii) AIBN, dioxane, 80 °C, 3 h; (iv) DMF, HCl, H_2O, 20 °C, 18 h; v) anhydrous DMF, D,L-lactide, DBU, 20 °C, 3 h; (vi) for ZBCPs: MPC, DMF/MeOH, ascorbic acid, $CuBr_2$, and TPMA, 20 °C, 18 h; (vi) for NBCP, PEG_9MA, DMF, ascorbic acid, $CuBr_2$, and TPMA, 20 °C, 18 h.

Table 1. Block Copolymer Characterization

polymer	m (LA)[a]	n (MPC)[a]	n (PEG)[a]	M_n(g/mol)[a]	w_{sc}, MPC/PEG[b]	p[c]	Đ[d]	C_{CMC} (nM)[e]
NBCP-SS	9	0	11	890,673	0.68	0.24	1.24	2.65
ZBCP-SS	9	19	0	902,237	0.69	0.11	1.21	1.76
ZBCP-MM	19	39	0	1,819,212	0.68	0.05	1.21	1.10
ZBCP-LL	33	58	0	2,823,946	0.65	0.03	1.27	1.04

[a]Determined by ^{1}H NMR. [b]Weight fraction of the hydrophilic block (PMPC or PEG) per side chain estimated as $M_{sc,\ PMPC\ or\ PEG}/(M_{sc,\ PMPC\ or\ PEG} + M_{sc,\ PLA})$. [c]Packing parameter. [d]Measured by gel permeation chromatography. [e]Determined by fluorescence spectroscopy using pyrene as a probe.

and centrifuged at 500g for 5 min to isolate red blood cells (RBCs). This washing step was repeated five times. The isolated RBCs were diluted to 20 mL with DPBS yielding a concentration of (1.18×10^8 cells/mL), and this suspension was directly utilized for hemolysis assay. To assess the hemolytic activity of zwitterionic bottlebrush micelles, 0.4 mL of a fresh RBC suspension was added to 0.6 mL of a micelle suspension at various concentrations. The final concentrations of micelles were 5, 10, 25, 50, 100, 200, and 1000 μg/mL, whereas the number of RBCs was maintained constant. DI water (+RBCs) and DPBS (+RBCs) were used as positive and negative controls, respectively. All samples were incubated at 37 °C for 3 h, after which time they were centrifuged at 10,010g for 5 min. 200 μL of supernatant was transferred to a 96-well plate. Hemoglobin absorbance was measured on a BMG Labtech FLUOstarOmega plate reader at 540 nm with 655 nm as the reference. Percent hemolysis was obtained according to

$$\text{percent hemolysis}(\%) = \frac{\text{sample abs} - \text{negative control abs}}{\text{positive control abs} - \text{negative control abs}} \times 100$$

RESULTS AND DISCUSSION

Molecular Design. In probing the effects of interfacial curvature of amphiphilic bottlebrushes on aggregate structure, Rzayev established that highly uniform spherical micelles result from amphiphiles with a packing parameter $p \approx 0.3$, as is the case for small molecule surfactants.[13] The packing parameter is defined in terms of the volume (v_t) and length (l_t) of the hydrophobic component, and the cross-sectional area of the hydrophilic/hydrophobic interface (a_{cr}) as, $p = v_t/l_t a_{cr}$. To target the formation of spherical assemblies, we synthesized a series of amphiphilic bottlebrushes consisting of a block of poly(D,L-lactide) [PLA] and a block of either poly(oligoethylene glycol methacrylate) [PEG_9MA] or PMPC. Bottlebrush diblocks were produced in keeping with the following molecular parameters: (i) the compositional asymmetry (hydrophobic/hydrophilic block ratio) was maintained constant at ~0.6, (ii) packing parameters were chosen to be $p < 0.3$, and (iii) the cross-sectional area of the interface was varied by modulating hydrophilic and hydrophobic side-chain lengths. The three zwitterionic bottlebrush copolymers (ZBCPs) examined are distinguished according to the latter parameter as those with short (ZBCP-SS), medium (ZBCP-MM), and long (ZBCP-LL) side-chains. A nonionic PEG-based bottlebrush copolymer (NBCP-SS) was designed as an analog of the short zwitterionic bottlebrush to represent conventional PEG surface chemistry for control experiments.

Polymer Synthesis and Characterization. Bottlebrush copolymers (BCPs) were produced using a combination of ring-opening and controlled radical polymerizations (Figure 1) and were characterized by proton nuclear magnetic resonance (^{1}H NMR) and gel permeation chromatography (GPC). Spectra and chromatograms of all materials are provided as the Supporting Information (Figures S1–S6). Briefly, BCP backbones were produced from the sequential reversible addition–fragmentation chain-transfer (RAFT) polymerization of glycidyl methacrylate (GMA) and 2-((2-bromo-2-methylpropanoyl)oxy)ethyl methacrylate (BIEM), with subsequent removal of the chain transfer agent followed by epoxide acidification (Figure 1). The resulting backbone consisted of 103 repeat units of GMA (i.e., 206 initiating sites for the ring-opening polymerization of D,L-lactide), and 105 initiating sites for the atom transfer radical polymerization (ATRP) of hydrophilic side-chains, either zwitterionic or nonionic (B4 in Figures S2 and S6). D,L-lactide was then polymerized from the macroinitiator, and PLA side-chain lengths (S, M, and L) were modulated according to the monomer:hydroxyl feed ratio (Table S1). MPC, or PEG_9MA, was subsequently polymerized by ATRP, and chain lengths were also controlled by the monomer:initiator feed ratio (Table S2). A summary of the characterization results for all BCPs, including conversion, degree of polymerization, molecular weight, and dispersity, is provided in Table S3.

https://doi.org/10.1021/acsami.4c10968
ACS Appl. Mater. Interfaces 2024, 16, 55118–55129

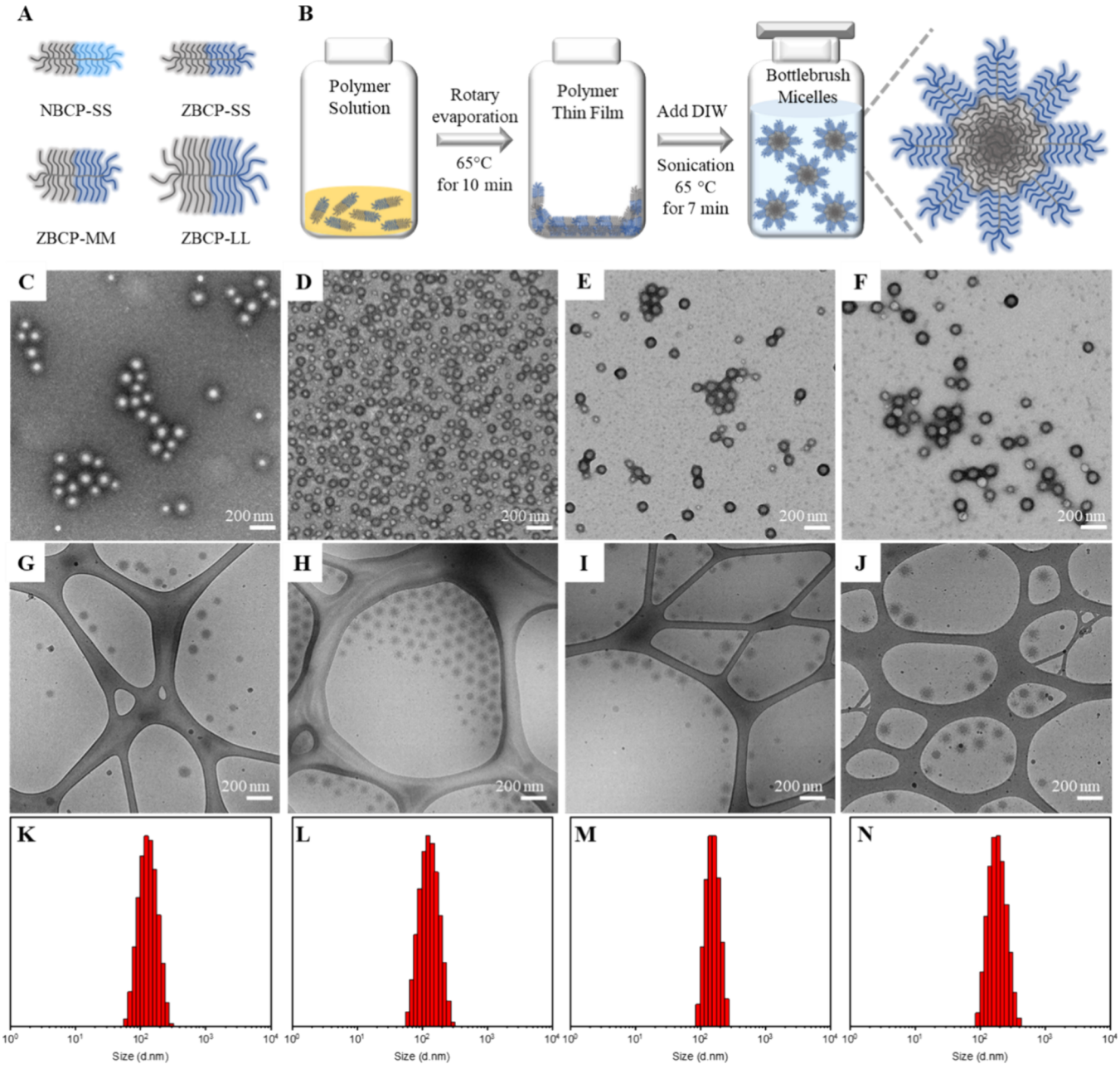

Figure 2. Characterization of nonionic and zwitterionic bottlebrush micelles. (A) Schematic of bottlebrush copolymers depicting the relative difference in side-chain lengths. (B) Illustration of the optimized micellization method by direct dissolution. (C–F) Representative transmission electron micrographs (TEMs). (G–J) Representative cryo-TEMs. (K–N) Size distributions measured by dynamic light scattering. Data correspond to N-SS (C, G, K), Z-SS (D, H, L), Z-MM (E, I, M), and Z-LL (F, J, N). All scale bars correspond to 200 nm. DLS data correspond to normalized intensity.

Table 2. Characterization of Bottlebrush Micelles

micelles	morphology[a]	D_{core} (nm)[b]	D_h (nm)[c]	PDI[c]	ζ potential[c]	N_{agg}[d]
N-SS	S	48.2 ± 10.9	124.1 ± 1.6	0.09	−5.8 ± 0.1	164
Z-SS	S	40.7 ± 6.1	120.4 ± 2.3	0.03	−7.7 ± 0.1	99
Z-MM	S	53.9 ± 9.4	133.3 ± 2.4	0.03	−2.8 ± 0.5	109
Z-LL	S	66.1 ± 9.9	165.8 ± 2.1	0.04	−0.5 ± 0.5	115

[a]Predominant morphology by cryo-TEM; S: sphere. [b]Measured from cryo-TEM images. [c]Measured by dynamic light scattering. [d]Estimated from the cryo-TEM core diameter and the melt density of PLA.

Following previous reports, the initiation efficiency for the ring-opening polymerization of D,L-lactide was estimated by ^{1}H NMR end-group analysis and was found to be nearly quantitative (>95%) for all copolymers (Figure S3). The grafting efficiencies of the hydrophilic blocks, relevant for estimating packing parameters, were not experimentally

https://doi.org/10.1021/acsami.4c10968
ACS Appl. Mater. Interfaces 2024, 16, 55118−55129

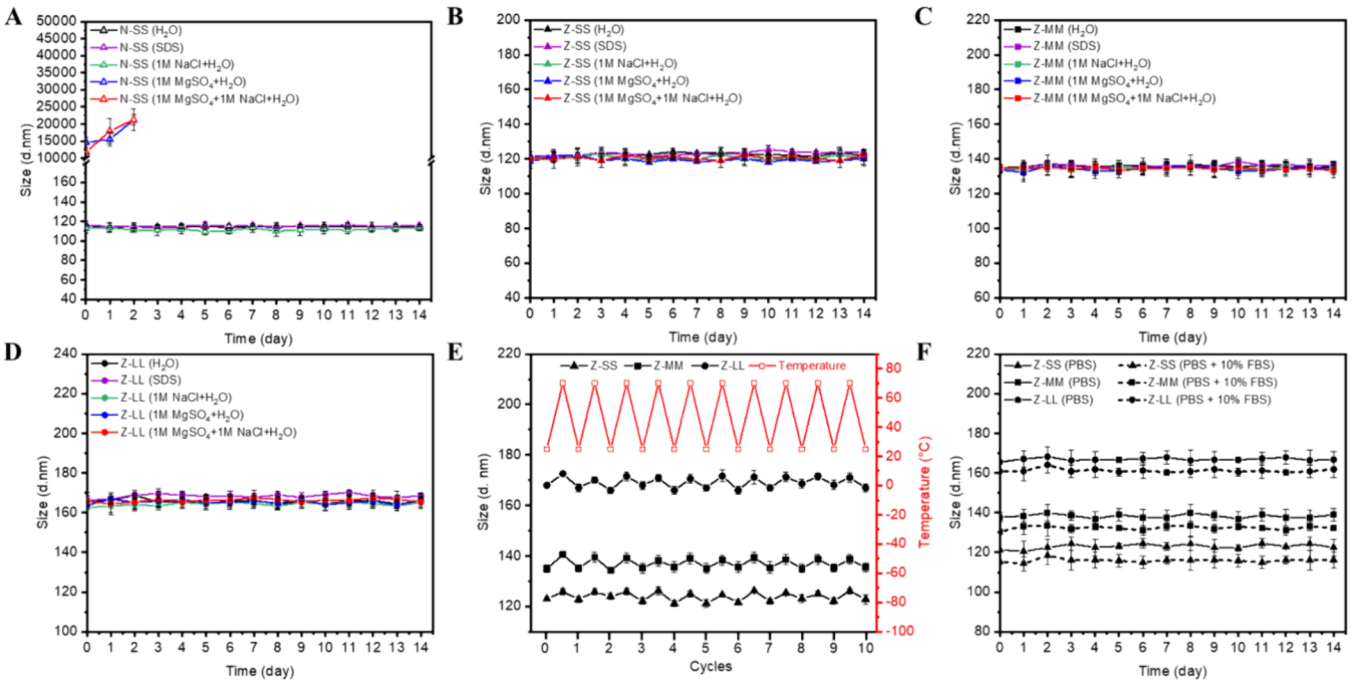

Figure 3. Evaluation of long-term colloidal stability and stability against the disassembly of zwitterionic and nonionic micelles. Shown are average hydrodynamic diameters of N-SS (A), Z-SS (B), Z-MM (C), and Z-LL (D) in 5 mg/mL sodium dodecyl sulfate (SDS), 1 M NaCl, 1 M $MgSO_4$, and 1 M NaCl + 1 M $MgSO_4$). Measurements were taken over 14 days. (E) Thermal stability of Z-SS, Z-MM and Z-LL for 10 cycles of temperature changes. (F) Long-term micellar stability of Z-SS, Z-MM and Z-LL in PBS, and PBS+10% FBS at 37 °C. DLS data correspond to normalized intensity.

measured; however, previous reports of bottlebrushes with ATRP-grafted side chains report initiation efficiencies ranging between 40 and 85% for methacrylate-based monomers.[39,54−57] Lower initiation efficiencies would lead to longer hydrophilic side chains, which would result in smaller packing parameters. Thus, even in the upper limit of 100% grafting efficiency, the resulting values of the packing parameters for nonionic and zwitterionic bottlebrushes are below 0.3 (Table 1), thus promoting the formation of spherical self-assemblies. C_{CMC} measurements revealed all BCPs had values in the nanomolar range, as previously reported for this class of polymeric surfactant.[13,58] As the length of the side chains increased from SS to LL, the hydrophilic fraction decreased slightly from 0.69 to 0.65, reflecting a corresponding increase in the hydrophobic fraction of the copolymer with longer side chains. This led to a reduction in the C_{CMC} values, attributed to enhanced hydrophobic interactions (Table 1 and Figure S7). A more dramatic polarity change between the hydrophobic and hydrophilic blocks is anticipated for the zwitterionic system compared to the nonionic one, which explains the higher C_{CMC} of NBCP-SS (2.7 nM) compared to ZBCP-SS (1.8 nM).

Aqueous Self-Assembly. NBCP-SS and ZBCPs were self-assembled into micelles following a direct dissolution method (Figure 2A,B). Micelles from NBCP-SS are labeled as N-SS, whereas zwitterionic micelles are identified according to the side-chain length of the BCPs as Z-SS, Z-MM, and Z-LL. Initial attempts at self-assembly were carried out following a previously published method,[13] which consisted of heating an aqueous solution of the BCPs to 65 °C and vigorously stirring this mixture overnight with the expectation of producing uniform micelles. This temperature was chosen to allow for increased mobility of the hydrophobic PLA segments (T_g = 48 °C) while remaining below the lower critical solution temperature of PEG_9MA (90 °C). Attempts with this procedure led to aggregates with broad particle size distributions and undesirable precipitates. The ultralow C_{CMC}, high molecular weights (~MDa), and structural rigidity of bottlebrush copolymers contribute to their limited mobility and difficulty in spontaneous self-assembly into uniform structures in aqueous solution with low energy input. To facilitate molecular reorganization, self-assembly was carried out by combining incubation at elevated temperature (65 °C) with brief sonication (7 min), resulting in well-controlled and highly uniform micelles with narrow size distributions (PDI < 0.045). The resulting micelles were characterized by dynamic light scattering (DLS), transmission electron microscopy (TEM), and cryo-TEM, as shown in Table 2 and Figure 2C−N.

Cryo-TEM imaging reveals large micellar assemblies with a dense, hydrophobic, spherical core but with individual bottlebrush hydrophilic chains protruding from the core and serving as corona chains. A similar morphology was observed between the N-SS and Z-SS samples. The spherical core particle with bottlebrush corona structure was the same across Z-SS, Z-MM, and Z-LL, while the size of the core increased from Z-SS (40.7 nm) to Z-LL (66.1 nm). Size distributions of micellar cores, measured from cryo-TEM images, are provided in Figure S10. In cryo-TEM, a minority of micelles exhibited either very short corona bottlebrushes or very few coronal bottlebrushes. This might be due to the inherent dispersity of the samples or to the presence of kinetically trapped assemblies, which will be discussed in detail in subsequent publications. Core diameters obtained from cryo-TEM images were also used to estimate micellar aggregation numbers, which, in the case of the zwitterionic series, increased with side-chain length.

https://doi.org/10.1021/acsami.4c10968
ACS Appl. Mater. Interfaces 2024, 16, 55118−55129

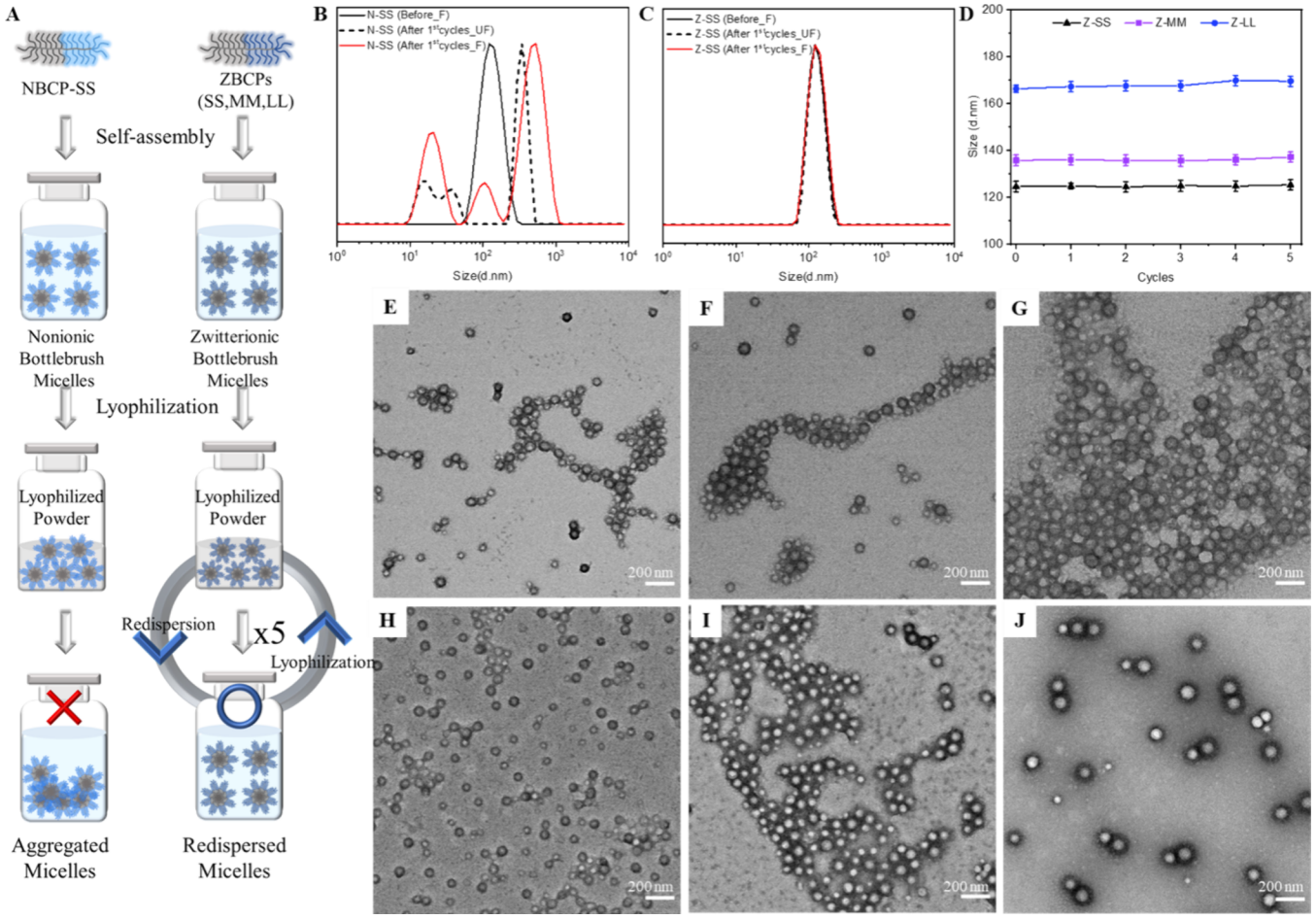

Figure 4. Characterization of redispersed nonionic and zwitterionic micelles. (A) Schematic illustration of the redispersion process. Particle size distributions of initial suspensions (solid black lines) and redispersed suspensions (solid red lines and dotted lines) of N-SS (B) and Z-SS (C). Filtered and unfiltered samples are identified as _F and _UF, respectively. (D) Average particle sizes, measured by DLS, after each of the five redispersion cycles of ZMs. Representative TEM images after the first (top row) and fifth (bottom row) redispersion cycles of Z-SS (E, H), Z-MM (F, I), and Z-LL (G, J). All scale bars correspond to 200 nm.

DLS data showed a gradual increase in micelle hydrodynamic diameter with side-chain length, from 120 (Z-SS) to 165 nm (Z-LL), whereas no appreciable difference was observed between the nonionic N-SS and the zwitterionic Z-SS micelles (124 nm vs 120 nm, respectively), the unimers of which had similar molecular weights. Overall, the hydrodynamic diameters of all micelles are within the range previously observed for PEG-based BCPs of similar structures and molecular weights ($D_h \approx 100-170$ nm).[13] The observed increase in micelle dimensions with side-chain length for the zwitterionic series can be attributed to a combination of chain stretching effects as well as higher aggregation numbers. Furthermore, all micelles showed slightly negative zeta potentials (∼−8 mV), indicating effective shielding of the negatively charged PLA core (∼−40 mV) by the net neutral zwitterionic layer. These values were also in good agreement with previously reported micelles from linear diblock copolymers of PLA-*b*-PMPC.

Colloidal Stability and Stability against Disassembly. To maximize therapeutic efficacy, polymeric micelles should exhibit great stability under various physiological conditions before drug delivery can be considered. Once introduced into the bloodstream, micelles undergo dissociation or aggregation due to dramatic dilution effects and/or interaction with salts or proteins present in biological environments. To examine the role of hydrophilic block chemistry on micellar stability, a systematic long-term evaluation of micelles from NBCP and ZBCPs was carried out in biologically relevant media and under conditions of high ionic strength.

Nonionic micelles (N-SS), and zwitterionic micelles (ZMs) were incubated in 1 M NaCl, 1 M $MgSO_4$, 1 M NaCl + 1 M $MgSO_4$, and sodium dodecyl sulfate (5 mg/mL) over 14 days at room temperature. Particle size was measured over this period and as shown in Figure 3A−D, excellent micellar stability was observed for the ZM series, which showed no change in particle size or dispersity regardless of the medium. In contrast, N-SS underwent strong aggregation in the presence of 1 M $MgSO_4$ and 1 M NaCl + 1 M $MgSO_4$. Turbidity measurements of ZMs showed >90% transmittance in all different ionic strength solutions, whereas the clear N-SS suspension immediately turned turbid with 70% transmittance in 1 M $MgSO_4$ and 1 M NaCl + 1 M $MgSO_4$ (Figure S8). These results are in line with our previous observations regarding changes in the structure of linear brushes of PMPC and PEG on flat surfaces despite the differences in chain architecture (linear chains vs bottlebrushes) and surface topography (smooth surfaces vs rough nanoparticles) between the two systems.[59,60] The noted invariability of ZM sizes and

https://doi.org/10.1021/acsami.4c10968
ACS Appl. Mater. Interfaces 2024, 16, 55118−55129

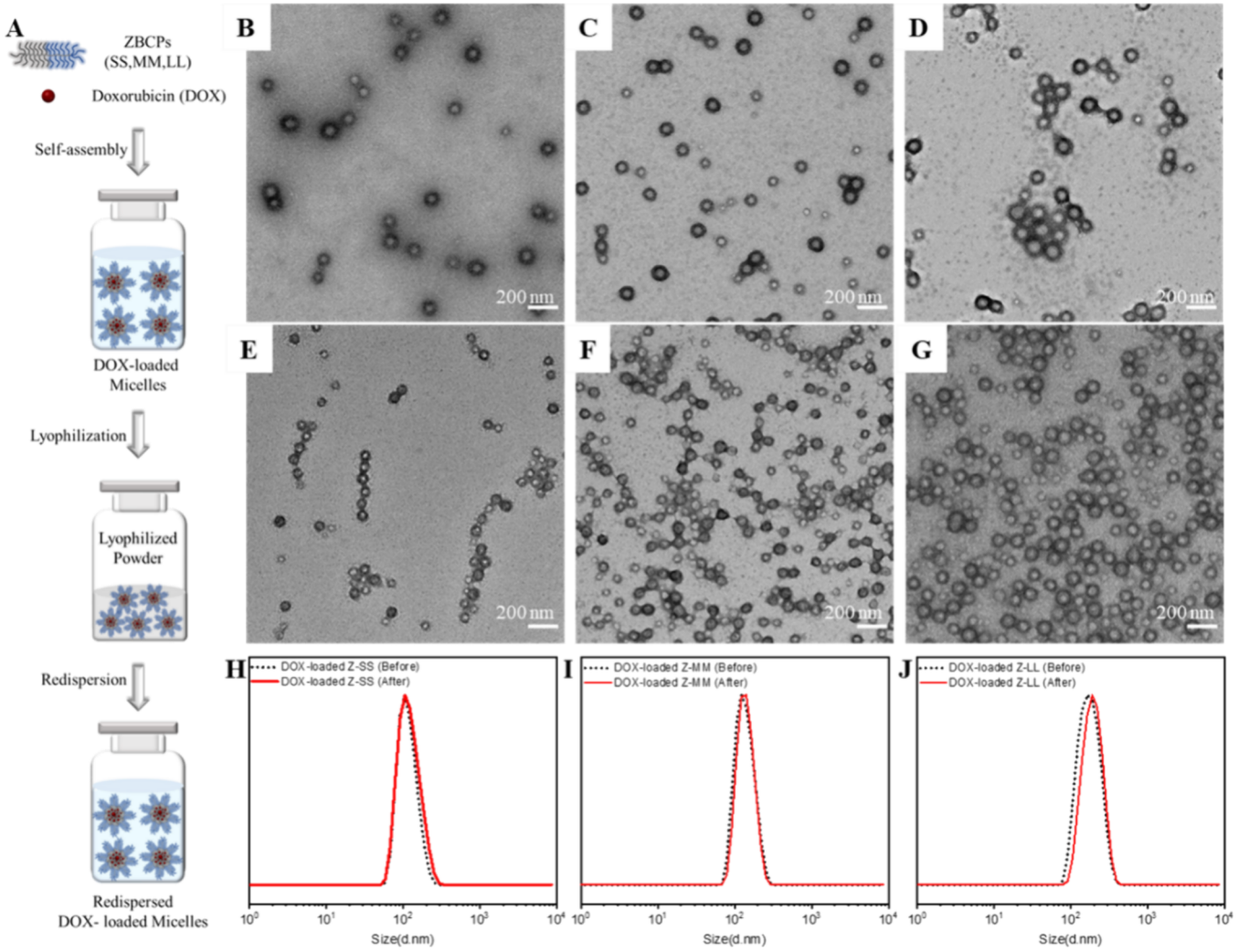

Figure 5. Redispersion properties of DOX-loaded zwitterionic bottlebrush micelles. (A) Schematic illustration of the redispersion process of DOX-loaded micelles. Representative TEM images of DOX-loaded Z-SS, Z-MM, and Z-LL micelles before redispersion (B–D). Representative TEM images of DOX-loaded Z-SS, Z-MM, and Z-LL micelles after redispersion (E–G). All scale bars correspond to 200 nm. (H–J) Size distributions of DOX-loaded micelles before (dotted black lines) and after (solid red lines) redispersion. Size distributions correspond to normalized volume intensities.

Table 3. Characterization of Doxorubicin-Loaded Zwitterionic Bottlebrush Micelles

DOX-loaded micelles	D_h (nm)[a]	PDI[a]	ζ potential[a]	DLC[b]	DLE[b]
Z-SS	121.2 ± 2.3	0.04	−7.3 ± 0.3	5.4 ± 0.1	56.7 ± 0.3
Z-MM	138.3 ± 2.6	0.03	−2.6 ± 0.2	7.3 ± 0.2	74.7 ± 0.3
Z-LL	167.8 ± 3.1	0.04	−0.6 ± 0.1	8.5 ± 0.1	86.1 ± 0.1

[a]Obtained from dynamic light scattering. [b]Measured by fluorescence spectroscopy.

size distributions at high salt concentrations is attributed to the strong solvation of PMPC by water, which dominates the dipolar screening, altered water structure, and competitive solute-water interactions existing under the examined conditions. This is not the case for PEG, which phase separates out of solution because of an alteration in the water structure in the presence of $MgSO_4$, resulting in colloidal instability for N-SS micelles.

Exposure to a high concentration of sodium dodecyl sulfate (5 mg/mL) produced no change in the particle size or dispersity over an extended period (14 days) regardless of hydrophilic block chemistry. The insolubility of N-SS or ZMs under these conditions is likely a result of high unimer interfacial tension and the large hydrophobic block molecular weight, yielding what appear to be frozen micelles, such that the reduction in interfacial tension necessary for solubilization to occur would likely be facilitated by addition of a cosolvent.

The thermal stability of ZMs was evaluated over 10 heating cycles, with temperatures cycling between 25 and 70 °C. While negligible size fluctuations were observed between each heating cycle (<3%, Figure 3E), all micelles show a slight increase in size with temperature. We attribute this to an increase in the solubility of the PMPC block as the temperature increases, resulting in chain extension of the backbone and MPC side chains. Lastly, ZMs incubated in PBS and PBS + 10% fetal bovine serum (FBS) also showed no

https://doi.org/10.1021/acsami.4c10968
ACS Appl. Mater. Interfaces 2024, 16, 55118−55129

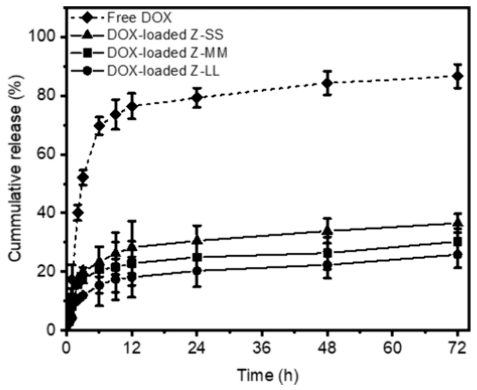

Figure 6. Release profile from DOX-loaded zwitterionic bottlebrush micelles in PBS at 37 °C for 72 h: Z-SS (triangles), Z-MM (squares), and Z-LL (circles). Dotted line represents free doxorubicin.

change in particle size and the absence of aggregates, as shown in Figure 3F.

Evaluation of Redispersed Micelles. Aqueous suspensions of N-SS and ZMs were subjected to lyophilization-dispersion cycles to validate their redispersibility in the absence of cryoprotectants (Figure 4A). Compared to N-SS, Z-SS exhibits nearly the same size and size distribution before and after redispersion, regardless of filtration (Figure 4B,C; Figure S9). All ZMs lyophilized into dry powders and exhibited great redispersibility even after 5 cycles, as verified by DLS and TEM, which clearly show they maintain their well-defined spherical morphology and narrow size distribution during this treatment (Figure 4D–J). In contrast, N-SS micelles were unable to redisperse even after one lyophilization cycle. These differences can be explained in terms of the stronger water affinity of the highly charged zwitterionic moieties compared to the nonionic PEG, yielding robust hydration shells that enable facile redispersion in the absence of cryoprotectants.

Evaluation of DOX-Loaded Micelles and In Vitro Release. Ultrastable ZMs were evaluated in terms of their ability to encapsulate the potent chemotherapeutic doxorubicin (DOX), the severe side-effects of which limit its application. DOX-loaded micelles were produced by the direct dissolution method previously described (Figure 5A). All loaded micelles maintained the well-defined spherical morphology and narrow size distribution of their unloaded analogs but were slightly larger (Table 3 and Figure 5B–J); for example, empty Z-SS was 133 nm, whereas the DOX-loaded Z-SS was 138 nm. Zeta potentials also remained unchanged before and after loading. Drug loading capacity (DLC) and drug loading efficiency (DLE) were evaluated for all ZMs and a consistent increase in DLC and DLE with side-chain length was noted. For example, DLC and DLE of Z-SS were 5.4 and 56.7% compared to those of Z-LL, which were 8.5 and 86.1%, respectively. These results showed a clear relationship between the size of the hydrophobic block and the drug loading ability of micelles. The redispersibility of lyophilized DOX-loaded ZMs was also evaluated, demonstrating that they maintained an intact morphology and size after redispersion with no evidence of aggregation (Figure 5H–J).

DOX-loaded ZMs were incubated in PBS (pH 7.4) for 72 h, and drug release was measured under sink conditions at predetermined time points. In general, delayed release kinetics were observed when comparing free DOX to micelle-loaded DOX (Figure 6), the kinetics of which varied with side-chain length. This effect is attributed to the size and surface area of the micelles as well as to their hydrophobic block size.

Hemolysis. Nanoparticle platforms considered for intravenous delivery must be assessed in terms of their interaction with—and potential destabilization of—red blood cells (RBC).[61−63] Therefore, a hemolysis assay was performed to evaluate the toxicity of ZMs toward RBC; hemocompatibility was examined for varying micelle concentrations up to ∼1000 μg/mL. As observed from Figure 7, compared to a positive control (+), RBC appeared to be relatively intact regardless of micelle size or concentration, showing a similar color of the supernatant to the negative control (−). While the larger ZMs consistently exhibited slightly higher percentages of hemolysis at all concentrations, very low membrane disruption was observed with a maximum of ∼8% hemolysis at 1000 μg/mL for the largest micelles (Z-LL). This result strongly supports

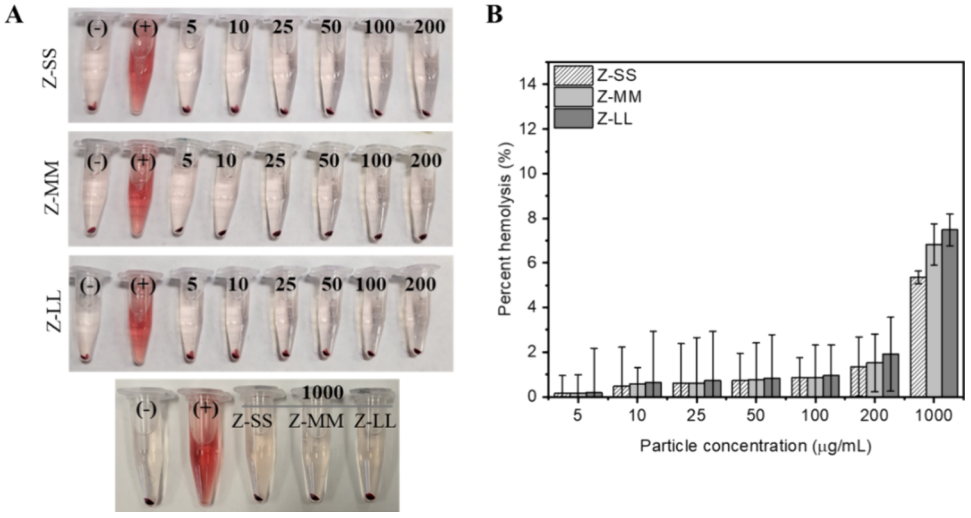

Figure 7. Hemolysis assay of the zwitterionic micelles. (A) Photographs of micelles at different concentrations with RBC solutions after centrifugation at 10,010 xg for 5 min. (−) and (+) symbols indicate negative control (PBS) and positive control (DIW), respectively. RBCs with membrane disruption release red hemoglobin to the supernatant at the positive control (+). (B) Percent hemolysis of Z-SS, Z-MM, and Z-LL at different concentrations (5 to 1000 μg/mL).

https://doi.org/10.1021/acsami.4c10968
ACS Appl. Mater. Interfaces 2024, 16, 55118−55129

ZMs as excellent candidates for intravenous delivery, given their great hemocompatibility. Further studies including *in vitro* and *in vivo* experiments are required to validate the pharmacodynamics and toxicology of ZMs to maximize their translational potential in clinical settings.

CONCLUSIONS

Amphiphilic nonionic (PEG) and zwitterionic (PMPC) bottlebrush copolymers were successfully synthesized using controlled radical and ring-opening polymerization methods. These amphiphilic bottlebrushes were self-assembled by a direct dissolution method using a combination of elevated temperature and sonication, and the resulting micelles—which exhibited very low dispersities—were examined in terms of their colloidal stability and integrity against disassembly. Zwitterionic micelles, in contrast to nonionic ones, were observed to have excellent colloidal stability in high ionic strength media and upon repeated cycles of lyophilization/resuspension, both of which were attributed to the robust solvation of phosphorylcholine moieties. Zwitterionic micelles were also observed to be stable at elevated temperatures and in the presence of 10% FBS. Modulating the micelle diameter was achieved by varying side-chain length, which also influenced the drug-loading ability and drug-release kinetics from zwitterionic micelles. The thermodynamic stability of the resulting micelles—attributed to the architecture of the unimers—along with the strong hydration shell of the phosphorylcholine moieties makes the hemocompatible zwitterionic bottlebrush copolymers examined herein excellent candidates for drug delivery and biological imaging applications and important alternatives to increasingly scrutinized PEG-based systems.

ASSOCIATED CONTENT

Supporting Information

The Supporting Information is available free of charge at https://pubs.acs.org/doi/10.1021/acsami.4c10968.

^{1}H NMR spectra, gel permeation chromatography, critical micelle concentration measurements, and core size distributions (PDF)

AUTHOR INFORMATION

Corresponding Author

Margarita Herrera-Alonso − *School of Materials Science and Engineering and Department of Chemical and Biological Engineering, Colorado State University, Fort Collins, Colorado 80523, United States;* orcid.org/0000-0002-6064-8699; Email: m.herrera-alonso@colostate.edu

Authors

Jeonghun Lee − *School of Materials Science and Engineering, Colorado State University, Fort Collins, Colorado 80523, United States;* orcid.org/0000-0002-9996-0110

Yao Tang − *Department of Materials Science and Engineering, University of Delaware, Newark, Delaware 19716, United States;* orcid.org/0000-0002-0917-3819

Karla E. Cureño Hernandez − *School of Materials Science and Engineering, Colorado State University, Fort Collins, Colorado 80523, United States;* orcid.org/0000-0002-1835-3678

Sunghoon Kim − *School of Materials Science and Engineering, Colorado State University, Fort Collins, Colorado 80523, United States;* orcid.org/0000-0002-1313-4951

Rahmi Lee − *Department of Biomedical Sciences, Colorado State University, Fort Collins, Colorado 80523, United States;* orcid.org/0000-0002-6955-1383

Zachary Cartwright − *School of Biomedical Engineering, Colorado State University, Fort Collins, Colorado 80523, United States;* orcid.org/0009-0009-0964-0948

Darrin J. Pochan − *Department of Materials Science and Engineering, University of Delaware, Newark, Delaware 19716, United States;* orcid.org/0000-0002-0454-2339

Complete contact information is available at: https://pubs.acs.org/10.1021/acsami.4c10968

Notes

The authors declare no competing financial interest.

REFERENCES

(1) Gao, H.; Matyjaszewski, K. Synthesis of Molecular Brushes by "Grafting onto" Method: Combination of ATRP and Click Reactions. *J. Am. Chem. Soc.* **2007**, *129* (20), 6633−6639.

(2) Xia, Y.; Olsen, B. D.; Kornfield, J. A.; Grubbs, R. H. Efficient Synthesis of Narrowly Dispersed Brush Copolymers and Study of Their Assemblies: The Importance of Side-Chain Arrangement. *J. Am. Chem. Soc.* **2009**, *131* (51), 18525−18532.

(3) Yuan, Y. Y.; Du, Q.; Wang, Y. C.; Wang, J. One-Pot Syntheses of Amphiphilic Centipede-like Brush Copolymers via Combination of Ring-Opening Polymerization and "Click" Chemistry. *Macromolecules* **2010**, *43* (4), 1739−1746.

(4) Chang, H. Y.; Lin, Y. L.; Sheng, Y. J.; Tsao, H. K. Multilayered Polymersome Formed by Amphiphilic Asymmetric Macromolecular Brushes. *Macromolecules* **2012**, *45* (11), 4778−4789.

(5) Rzayev, J. Molecular Bottlebrushes: New Opportunities in Nanomaterials Fabrication. *ACS Macro Lett.* **2012**, *1* (9), 1146−1149.

(6) Cheng, C.; Khoshdel, E.; Wooley, K. L. Facile one-pot synthesis of brush polymers through tandem catalysis using Grubbs' catalyst for both ring-opening metathesis and atom transfer radical polymerizations. *Nano Lett.* **2006**, *6* (8), 1741−1746.

(7) Li, Z.; Ma, J.; Cheng, C.; Zhang, K.; Wooley, K. L. Synthesis of Hetero-Grafted Amphiphilic Diblock Molecular Brushes and Their Self-Assembly in Aqueous Medium. *Macromolecules* **2010**, *3* (43), 1182−1184.

(8) Huang, K.; Rzayev, J. Charge and Size Selective Molecular Transport by Amphiphilic Organic Nanotubes. *J. Am. Chem. Soc.* **2011**, *133* (42), 16726−16729.

(9) Huang, K.; Jacobs, A.; Rzayev, J. De novo synthesis and cellular uptake of organic nanocapsules with tunable surface chemistry. *Biomacromolecules* **2011**, *12* (6), 2327.

(10) Li, A.; Ma, J.; Sun, G. R.; Li, Z.; Cho, S. H.; Clark, C.; Wooley, K. L. One-pot, facile synthesis of well-defined molecular brush copolymers by a tandem RAFT and ROMP, "Grafting-through" strategy. *J. Polym. Sci. Pol Chem.* **2012**, *50* (9), 1681−1688.

(11) Sun, G. R.; Cho, S. H.; Clark, C.; Verkhoturov, S. V.; Eller, M. J.; Li, A.; Pavia-Jimenez, A.; Schweikert, E. A.; Thackeray, J. W.; Trefonas, P.; et al. Nanoscopic Cylindrical Dual Concentric and Lengthwise Block Brush Terpolymers as Covalent Preassembled High-Resolution and High-Sensitivity Negative-Tone Photoresist Materials. *J. Am. Chem. Soc.* **2013**, *135* (11), 4203−4206.

(12) Chremos, A.; Theodorakis, P. E. Morphologies of Bottle-Brush Block Copolymers. *ACS Macro Lett.* **2014**, *3* (10), 1096−1100.

(13) Fenyves, R.; Schmutz, M.; Horner, I. J.; Bright, F. V.; Rzayev, J. Aqueous Self-Assembly of Giant Bottlebrush Block Copolymer Surfactants as Shape-Tunable Building Blocks. *J. Am. Chem. Soc.* **2014**, *136* (21), 7762−7770.

(14) Ahmed, E.; Womble, C. T.; Weck, M. Synthesis and Aqueous Self-Assembly of ABCD Bottlebrush Block Copolymers. *Macromolecules* **2020**, *53* (20), 9018−9025.
(15) Alaboalirat, M.; Qi, L. Q.; Arrington, K. J.; Qian, S.; Keum, J. K.; Mei, H.; Littrell, K. C.; Sumpter, B. G.; Carrillo, J. M. Y.; Verduzco, R.; et al. Amphiphilic Bottlebrush Block Copolymers: Analysis of Aqueous Self-Assembly by Small-Angle Neutron Scattering and Surface Tension Measurements. *Macromolecules* **2019**, *52* (2), 465−476.
(16) Hassler, J. F.; Van Zee, N. J.; Crabtree, A. A.; Bates, F. S.; Hackel, B. J.; Lodge, T. P. Synthesis and Micellization of Bottlebrush Poloxamers. *ACS Macro Lett.* **2022**, *11* (4), 460−467.
(17) Grundler, J.; Shin, K.; Suh, H. W.; Zhong, M. J.; Saltzman, W. M. Surface Topography of Polyethylene Glycol Shell Nanoparticles Formed from Bottlebrush Block Copolymers Controls Interactions with Proteins and Cells. *ACS Nano* **2021**, *15* (10), 16118−16129.
(18) Mullner, M. Molecular polymer bottlebrushes in nanomedicine: therapeutic and diagnostic applications. *Chem. Commun.* **2022**, *58* (38), 5683−5716.
(19) Mullner, M. Molecular Polymer Brushes in Nanomedicine. *Macromol. Chem. Phys.* **2016**, *217* (20), 2209−2222.
(20) Unsal, H.; Onbulak, S.; Calik, F.; Er-Rafik, M.; Schmutz, M.; Sanyal, A.; Rzayev, J. Interplay between Molecular Packing, Drug Loading, and Core Cross-Linking in Bottlebrush Copolymer Micelles. *Macromolecules* **2017**, *50* (4), 1342−1352.
(21) Synatschke, C. V.; Nomoto, T.; Cabral, H.; Fortsch, M.; Toh, K.; Matsumoto, Y.; Miyazaki, K.; Hanisch, A.; Schacher, F. H.; Kishimura, A.; et al. Multicompartment Micelles with Adjustable Poly(ethylene glycol) Shell for Efficient in Vivo Photodynamic Therapy. *ACS Nano* **2014**, *8* (2), 1161−1172.
(22) Braga, C. B.; Pilli, R. A.; Ornelas, C.; Weck, M. Near-Infrared Fluorescent Micelles from Poly(norbornene) Brush Triblock Copolymers for Nanotheranostics. *Biomacromolecules* **2021**, *22* (12), 5290−5306.
(23) Vohidov, F.; Milling, L. E.; Chen, Q. X.; Zhang, W. X.; Bhagchandani, S.; Nguyen, H. V. T.; Irvine, D. J.; Johnson, J. A. ABC triblock bottlebrush copolymer-based injectable hydrogels: design, synthesis, and application to expanding the therapeutic index of cancer immunochemotherapy. *Chem. Sci.* **2020**, *11* (23), 5974−5986.
(24) Mullner, M.; Muller, A. H. E. Cylindrical polymer brushes - Anisotropic building blocks, unimolecular templates and particulate nanocarriers. *Polymer* **2016**, *98*, 389−401.
(25) Zou, J.; Zhang, S. Y.; Shrestha, R.; Seetho, K.; Donley, C. L.; Wooley, K. L. pH-Triggered reversible morphological inversion of orthogonally-addressable poly(3-acrylamidophenylboronic acid)-block-poly(acrylamidoethylamine) micelles and their shell crosslinked nanoparticles. *Polym. Chem.* **2012**, *3* (11), 3146−3156.
(26) Weaver, J. V. M.; Armes, S. P.; Butun, V. Synthesis and aqueous solution properties of a well-defined thermo-responsive schizophrenic diblock copolymer. *Chem. Commun.* **2002**, *18*, 2122−2123.
(27) Butun, V.; Lowe, A. B.; Billingham, N. C.; Armes, S. P. Synthesis of zwitterionic shell cross-linked micelles. *J. Am. Chem. Soc.* **1999**, *121* (17), 4288−4289.
(28) Zhang, Q.; Remsen, E. E.; Wooley, K. L. Shell cross-linked nanoparticles containing hydrolytically degradable, crystalline core domains. *J. Am. Chem. Soc.* **2000**, *122* (15), 3642−3651.
(29) Fujii, S.; Cai, Y. L.; Weaver, J. V. M.; Armes, S. P. Syntheses of shell cross-linked micelles using acidic ABC triblock copolymers and their application as pH-responsive particulate emulsifiers. *J. Am. Chem. Soc.* **2005**, *127* (20), 7304−7305.
(30) Read, E. S.; Armes, S. P. Recent advances in shell cross-linked micelles. *Chem. Commun.* **2007**, *29*, 3021−3035.
(31) Elsabahy, M.; Zhang, S.; Zhang, F.; Deng, Z. J.; Lim, Y. H.; Wang, H.; Parsamian, P.; Hammond, P. T.; Wooley, K. L. Surface Charges and Shell Crosslinks Each Play Significant Roles in Mediating Degradation, Biofouling, Cytotoxicity and Immunotoxicity for Polyphosphoester-based Nanoparticles. *Sci. Rep.* **2013**, *3*, No. 3313.
(32) Zhang, F. W.; Elsabahy, M.; Zhang, S. Y.; Lin, L. Y.; Zou, J.; Wooley, K. L. Shell crosslinked knedel-like nanoparticles for delivery of cisplatin: effects of crosslinking. *Nanoscale* **2013**, *5* (8), 3220−3225.
(33) Lee, J.; Hernandez, K. C.; Kim, S.; Herrera-Alonso, M. Solute Stabilization Effects of Nanoparticles Containing Boronic Acids in the Absence of Binding Pairs. *Langmuir* **2023**, *39*, 15328.
(34) Estephan, Z. G.; Schlenoff, P. S.; Schlenoff, J. B. Zwitteration As an Alternative to PEGylation. *Langmuir* **2011**, *27* (11), 6794−6800.
(35) Papi, M.; Pozzi, D.; Palmieri, V.; Caracciolo, G. Principles for optimization and validation of mRNA lipid nanoparticle vaccines against COVID-19 using 3D bioprinting. *Nano Today* **2022**, *43*, No. 101403.
(36) Stengel, D.; Demirel, B. H.; Knoll, P.; Truszkowska, M.; Laffleur, F.; Bernkop-Schnürch, A. PEG vs. zwitterions: How these surface decorations determine cellular uptake of lipid-based nanocarriers. *J. Colloid Interface Sci.* **2023**, *647*, 52−64.
(37) Zhou, L. Y.; Zhu, Y. H.; Wang, X. Y.; Shen, C.; Wei, X. W.; Xu, T.; He, Z. Y. Novel zwitterionic vectors: Multi-functional delivery systems for therapeutic genes and drugs. *Computational and Structural Biotechnology Journal* **2020**, *18*, 1980−1999.
(38) Zeng, Z.; Chen, S.; Chen, Y. Zwitterionic Polymer: A New Paradigm for Protein Conjugation beyond PEG. *ChemMedChem* **2023**, *18* (20), No. e202300245.
(39) Takano, S.; Islam, W.; Nakazawa, K.; Maeda, H.; Sakurai, K.; Fujii, S. Phosphorylcholine-Grafted Molecular Bottlebrush-Doxorubicin Conjugates: High Structural Stability, Long Circulation in Blood, and Efficient Anticancer Activity. *Biomacromolecules* **2021**, *22* (3), 1186−1196.
(40) Rajan, R.; Matsumura, K. A zwitterionic polymer as a novel inhibitor of protein aggregation. *J. Mater. Chem. B* **2015**, *3* (28), 5683−5689.
(41) Liu, M.; Zhang, X.; Guo, H.; Zhu, Y.; Wen, C.; Sui, X.; Yang, J.; Zhang, L. Dimethyl Sulfoxide-Free Cryopreservation of Chondrocytes Based on Zwitterionic Molecule and Polymers. *Biomacromolecules* **2019**, *20* (10), 3980−3988.
(42) Yamasaki, R.; Rajan, R.; Matsumura, K. Enhancement of cryopreservation with intracellularly permeable zwitterionic polymers. *Chem. Commun.* **2023**, *59* (94), 14001−14004.
(43) Lenders, V.; Koutsoumpou, X.; Phan, P.; Soenen, S. J.; Allegaert, K.; de Vleeschouwer, S.; Toelen, J.; Zhao, Z. M.; Manshian, B. B. Modulation of engineered nanomaterial interactions with organ barriers for enhanced drug transport. *Chem. Soc. Rev.* **2023**, *52* (14), 4672−4724.
(44) Xiang, Y.; Xu, R. G.; Leng, Y. S. Molecular Simulations of the Hydration Behavior of a Zwitterion Brush Array and Its Antifouling Property in an Aqueous Environment. *Langmuir* **2018**, *34* (6), 2245−2257.
(45) Kato, Y.; Uto, T.; Tanaka, D.; Ishibashi, K.; Kobayashi, A.; Hazawa, M.; Wong, R. W.; Ninomiya, K.; Takahashi, K.; Hirata, E.; et al. Synthetic zwitterions as efficient non-permeable cryoprotectants. *Commun. Chem.* **2021**, *4* (1), 151.
(46) Jung, S.; Park, K.; Park, S.; Heo, J.; Choi, W.; Hong, J. Unraveling the Structured Solvation Shell of Zwitterion Nanoparticles for Controlled Release of Nitric Oxide. *ACS Appl. Mater. Interfaces* **2021**, *13* (45), 54363−54374.
(47) Stals, P. J. M.; Li, Y. C.; Burdynska, J.; Nicolay, R.; Nese, A.; Palmans, A. R. A.; Meijer, E. W.; Matyjaszewski, K.; Sheiko, S. S. How Far Can We Push Polymer Architectures? *J. Am. Chem. Soc.* **2013**, *135* (31), 11421−11424.
(48) Aguirre-Chagala, Y. E.; Santos, J. L.; Aguilar-Castillo, B. A.; Herrera-Alonso, M. Synthesis of Copolymers from Phenylboronic Acid-Installed Cyclic Carbonates. *ACS Macro Lett.* **2014**, *3* (4), 353−358.
(49) Luo, H. Y.; Szymusiak, M.; Garcia, E. A.; Lock, L. L.; Cui, H. G.; Liu, Y.; Herrera-Alonso, M. Solute-Triggered Morphological Transitions of an Amphiphilic Heterografted Brush Copolymer as a Single-Molecule Drug Carrier. *Macromolecules* **2017**, *50* (5), 2201−2206.
(50) Luo, Y.; Yin, X.; Yin, X.; Chen, A.; Zhao, L.; Zhang, G.; Liao, W.; Huang, X.; Li, J.; Zhang, C. Y. Dual pH/Redox-Responsive Mixed

Polymeric Micelles for Anticancer Drug Delivery and Controlled Release. *Pharmaceutics* **2019**, *11* (4), No. 176.
(51) Zhang, C. Y.; Yang, Y. Q.; Huang, T. X.; Zhao, B.; Guo, X. D.; Wang, J. F.; Zhang, L. J. Self-assembled pH-responsive MPEG-b-(PLA-co-PAE) block copolymer micelles for anticancer drug delivery. *Biomaterials* **2012**, *33* (26), 6273−6283.
(52) Dobrovoiskaia, M. A.; Clogston, J. D.; Neun, B. W.; Hall, J. B.; Patri, A. K.; McNeil, S. E. Method for analysis of nanoparticle hemolytic properties in vitro. *Nano Lett.* **2008**, *8* (8), 2180−2187.
(53) Liao, K. H.; Lin, Y. S.; Macosko, C. W.; Haynes, C. L. Cytotoxicity of Graphene Oxide and Graphene in Human Erythrocytes and Skin Fibroblasts. *ACS Appl. Mater. Interfaces* **2011**, *3* (7), 2607−2615.
(54) Fujii, S.; Takano, S.; Nakazawa, K.; Sakurai, K. Impact of Zwitterionic Polymers on the Tumor Permeability of Molecular Bottlebrush-Based Nanoparticles. *Biomacromolecules* **2022**, *23*, 2846.
(55) Neugebauer, D.; Sumerlin, B. S.; Matyjaszewski, K.; Goodhart, B.; Sheiko, S. S. How dense are cylindrical brushes grafted from a multifunctional macroinitiator? *Polymer* **2004**, *45* (24), 8173−8179.
(56) Sumerlin, B. S.; Neugebauer, D.; Matyjaszewski, K. Initiation efficiency in the synthesis of molecular brushes by grafting from via atom transfer radical polymerization. *Macromolecules* **2005**, *38* (3), 702−708.
(57) Burdynska, J.; Daniel, W.; Li, Y. C.; Robertson, B.; Sheiko, S. S.; Matyjaszewski, K. Molecular Bottlebrushes with Bimodal Length Distribution of Side Chains. *Macromolecules* **2015**, *48* (14), 4813−4822.
(58) Pesek, S. L.; Li, X. Y.; Hammouda, B.; Hong, K. L.; Verduzco, R. Small-Angle Neutron Scattering Analysis of Bottlebrush Polymers Prepared via Grafting-Through Polymerization. *Macromolecules* **2013**, *46* (17), 6998−7005.
(59) Petroff, M. G.; Garcia, E. A.; Herrera-Alonso, M.; Bevan, M. A. Ionic Strength-Dependent Interactions and Dimensions of Adsorbed Zwitterionic Copolymers. *Langmuir* **2019**, *35* (14), 4976−4985.
(60) Jumai'an, E.; Garcia, E.; Herrera-Alonso, M.; Bevan, M. A. Specific Ion Effects on Adsorbed Zwitterionic Copolymers. *Macromolecules* **2020**, *53* (22), 9769−9778.
(61) Bao, H.; Wang, N.; Chen, S.; Wang, Y.; Shao, H. B.; Ni, Y. C.; Li, Y. K.; Liu, X.; Han, X. J. Multimodal Theranostic Nanoparticles for Necrosis Targeting, Fluorescence/SPECT Imaging, and Radiotherapy of Residual Tumors after Hepatocellular Carcinoma Ablation. *Mol. Pharmaceutics* **2024**, *21* (4), 1729−1744.
(62) Chen, L. Y.; Simpson, J. D.; Fuchs, A. V.; Rolfe, B. E.; Thurecht, K. J. Effects of Surface Charge of Hyperbranched Polymers on Cytotoxicity, Dynamic Cellular Uptake and Localization, Hemotoxicity, and Pharmacokinetics in Mice. *Mol. Pharmaceutics* **2017**, *14* (12), 4485−4497.
(63) Han, X.; Taratula, O.; Taratula, O.; Xu, K.; St Lorenz, A.; Moses, A.; Jahangiri, Y.; Yu, G.; Farsad, K. Biodegradable Hypericin-Containing Nanoparticles for Necrosis Targeting and Fluorescence Imaging. *Mol. Pharmaceutics* **2020**, *17* (5), 1538−1545.

https://doi.org/10.1021/acsami.4c10968
ACS Appl. Mater. Interfaces 2024, 16, 55118−55129